ACTA ONCOLOGICA
2019, VOL. 58, NO. 10, 1536–1539
https://doi.org/10.1080/0284186X.2019.1631477

Taylor & Francis
Taylor & Francis Group

LETTER TO THE EDITOR

Predicting late magnetic resonance image changes in glioma patients after proton therapy

J. Eulitz[a,b,c,d], E.G.C. Troost[a,b,c,d,e,f,g,h,i], F. Raschke[a,b,d], E. Schulz[a,b,d], B. Lutz[j], A. Dutz[a,b,d], S. Löck[a,b,d,f,i], P. Wohlfahrt[k*], W. Enghardt[a,b,c,d,f,i], C. Karpowitz[a,b,c,d,e,f,g,h,i], M. Krause[a,b,c,d,e,f,g,h,i] and A. Lühr[a,b,d,f,i]

[a]OncoRay – National Center for Radiation Research in Oncology, Faculty of Medicine, Dresden, Germany; [b]University Hospital Carl Gustav Carus, Technische Universität Dresden, Helmholtz-Zentrum Dresden-Rossendorf, Dresden, Germany; [c]Department of Radiotherapy and Radiation Oncology, Faculty of Medicine, University Hospital Carl Gustav Carus, Technische Universität Dresden, Dresden, Germany; [d]Helmholtz-Zentrum Dresden-Rossendorf, Institute of Radiooncology – OncoRay, Dresden, Germany; [e]National Center for Tumor Diseases (NCT), Partner Site Dresden, Dresden, Germany; [f]German Cancer Research Center (DKFZ), Heidelberg, Germany; [g]Faculty of Medicine, University Hospital Carl Gustav Carus, Technische Universität Dresden, Dresden, Germany; [h]Helmholtz Association/Helmholtz-Zentrum Dresden-Rossendorf (HZDR), Dresden, Germany; [i]German Cancer Consortium (DKTK), Partner Site Dresden, Heidelberg, Germany; [j]Helmholtz-Zentrum Dresden-Rossendorf, Institute for Radiation Physics, Dresden, Germany; [k]Department of Radiation Oncology, Massachusetts General Hospital and Harvard Medical School, Boston, MA, USA

ARTICLE HISTORY Received 2 April 2019; Accepted 31 May 2019

Introduction

Proton beam therapy (PBT) is expected to reduce radiation-induced side-effects compared to state-of-the-art photon treatments as the physical properties of protons offer the possibility to spare normal tissues surrounding the tumor from the dose [1]. However, irradiation of normal tissue cannot be fully avoided and may lead to long-term adverse effects. Severe normal tissue complications of the central nervous system (CNS) can be characterized by contrast enhancement (CE) on post-treatment magnetic resonance images (MRI) [2] corresponding to a breakdown of the blood–brain barrier. There is increasing evidence of a regional variation in susceptibility to radiation-dependent normal brain tissue damage [3,4]. Furthermore, recent findings suggest a variable relative biological effectiveness (RBE) [5] for proton therapy of the brain which translates into regional variations in radiation effect – a topic of intense discussion [6]. Since PBT can be delivered with high local precision, there is a demand for radiation response models identifying brain regions with increased risk for developing late radiation damage.

In our clinic, late CE occurs in brain tissue for glioma patients often within the periventricular region (PVR). As the ventricular liquor contains no vascular structures, the PVR may be, in particular, disadvantaged considering vascular supply and thus more vulnerable for developing late brain injury. However, so far the PVR has not been evaluated in normal tissue response models for proton therapy.

Based on six glioma patients, this study aims to identify relevant anatomical and physical parameters which may explain the spatial heterogeneity of late brain toxicities after proton therapy.

Methods

Study design

Six glioma patients (1/5 grade II/III) treated with adjuvant radio(chemo)therapy using passively scattered protons at the University Proton Therapy Dresden (UPTD) between September 2015 and August 2017 were evaluated. All the patients showed contrast enhancement on follow-up T1-weighted (T1w-CE) MRI, corresponding to treatment-related changes. This was confirmed using either histology (4/6 patients) or radiological diagnosis (2/6 patients). Grade III glioma patients were treated to a total dose of 60 Gy in 30 fractions, whereas the total dose in grade II glioma patients was 54 Gy in 27 fractions. Patient and treatment characteristics are shown in Supplementary Tables S1 and S2, respectively.

Image acquisition and processing

T1-weighted MRIs after contrast injection were taken from clinical magnetic resonance (MR) exams acquired as part of standard patient care. Acquisition parameters are summarized in Supplementary Table S1. Image changes were

CONTACT Jan Eulitz Jan.Eulitz@uniklinikum-dresden.de OncoRay, National Center for Radiation Research in Oncology, Händelallee 26, Dresden 01309, Germany

Supplemental data for this article can be accessed here.

*Patrick Wohlfahrt is currently working as a postdoc at the Department of Radiation Oncology at the Massachusetts General Hospital in Boston.

This article has been republished with minor changes. These changes do not impact the academic content of the article.

manually contoured on the earliest available T1w-CE follow-up MR images (fuMRI) that show contrast. For one patient, the earliest fuMRI with image changes had a slice thickness of 5 mm and was unsuitable for accurate image processing. Hence, the subsequent fuMRI with a slice thickness of 2 mm was used instead.

These contour masks were non-linearly coregistered to the T1w-CE planning MRI (pMRI) [7]. The lateral ventricles were segmented on the pMRI using an in-house developed image segmentation framework. The periventricular region (PVR) was defined as a band around the segmented ventricles with a 4 mm extension, which was taken from [8]. All image change contours and masks were transferred to the pCT for further analysis by rigid coregistration of the pMRI to the pCT.

Statistical analysis

For statistical analysis, only brain tissue voxels were incorporated that received more than 2% of the prescribed dose. Furthermore, cerebrospinal fluid (CSF) voxels were excluded, as no image changes related to normal brain tissue complication were expected in these regions. Image voxels within the delineated T1w-CE region were labeled as 1; the remaining voxels were set to 0. The same labeling procedure was applied for the delineated PVR.

Dose and LET simulations were performed on a high-performance computation cluster using an in-house developed MC simulation framework [9] based on the MC tool TOPAS [10]. For LET calculation, the default TOPAS proton LET (track-averaged) scorer was used [11,12]. Ten voxel-wise logit models were built based on the variables dose, LET, the PVR contour as well as the interaction terms dose $\times$ LET and dose $\times$ PVR. Intercorrelation among the variables was tested by calculating the Spearman rank coefficient.

Leave-one-out cross validation (LOOCV) was performed to evaluate the variance and robustness of the models regarding patient variability. In each of the six cross-validation folds, a different patient was removed from the dataset, a model was developed on the remaining five patients and validated on the left-out patient by assessing the area under the curve (AUC) of the receiver-operating characteristic (ROC).

The probability for an image change in a voxel was estimated by

$$P_{IC} = \frac{1}{1 + e^{-(\beta_0 + \vec{\beta}\vec{X})}}, \quad (1)$$

with model predictors $\vec{X}$ (dose, LET, PVR), coefficients $\vec{\beta}$ and constant β_0.

The coefficients were derived based on the voxel dataset from all six patients using python statsmodels library [13]. Additionally, the Akaike information criteria (AIC) and pseudo R-squared values were calculated for each model.

The TD_{15} dose, at which 15% of tissue voxels are predicted to show image changes, as function of LET was determined for the models. RBE values for 15% iso-effect were estimated from the TD_{15} data as,

$$RBE = \frac{TD_{15}\ (LET = 1.0\ keV/\mu m)}{TD_{15}\ (LET)}, \quad (2)$$

using TD_{15} at an LET of 1.0 keV/μm as the dose of a reference radiation.

Results

The intercorrelation between the variables dose, LET, dose times LET and the PVR was low to moderate with Spearman rank coefficients ranging from -0.58 to 0.54 (Supplementary Figure S1). The spatial distribution of the T1w-CE MR image changes in the brain was highly non-uniform occurring predominantly outside but close to the CTV (Figure 1).

The multivariable models $\mathcal{M}_{VIII}$, $\mathcal{M}_{IX}$, and $\mathcal{M}_{X}$ incorporating the predictors' dose, LET and the PVR revealed the highest average cross-validated AUC, the lowest AIC and highest pseudo-R-squared values (Table 1 and Supplementary Figure S2). Model calibration was reasonable up to about 15% (Supplementary Figure S3). The estimated TD_{15}(LET) and RBE(LET) values decreased and increased, respectively, with increasing LET (Supplementary Figure S4).

For model $\mathcal{M}_{X}$ with minimal AIC, the predicted image change probability is visualized for each patient on pMRI slices with T1w-CE contours that were deformable co-registered from fuMRI (Figure 1).

Discussion

This study establishes a radiobiological model approach to predict the observed highly non-uniform clinical radiation response in the brain after proton treatment. Damaged brain tissue regions were discriminated from non-contrast-receiving brain areas by using a combination of dose, LET and the PVR with cross-validated mean AUC values >0.9. The modeled tissue tolerance dose TD_{15} decreased with increasing LET, which indicates a variable proton RBE that increases with LET. The lower TD_{15} values obtained within the PVR may suggest an increased radiosensitivity of the PVR.

The multivariable logistic regression models with dose and LET ($\mathcal{M}_{VI}$, $\mathcal{M}_{VII}$) predicted the late image changes with high cross-validated AUC values of 0.88. In contrast, the univariable models with either dose or LET as predictor were poorly correlated with the image changes. This is another strong indication for clinical RBE variability with LET confirming the growing awareness of this effect [14].

The best image change prediction was achieved with the inclusion of the PVR both in cross-validated AUC values and in AIC and pR^2 measures. This has been confirmed in a LOOCV with 30 randomly selected non-overlapping voxel subsets (Supplementary Table S3).

The model parameter of the PVR predictor remained essentially unchanged for different models (Supplementary Table S4) and the PVR predictor performed best in univariable analysis. This may indicate an increased radio-sensitivity of the PVR for glioma patients with high risk to develop late brain injury. Further validation is required to assess the influence of the PVR in more detail. As the photon LET is

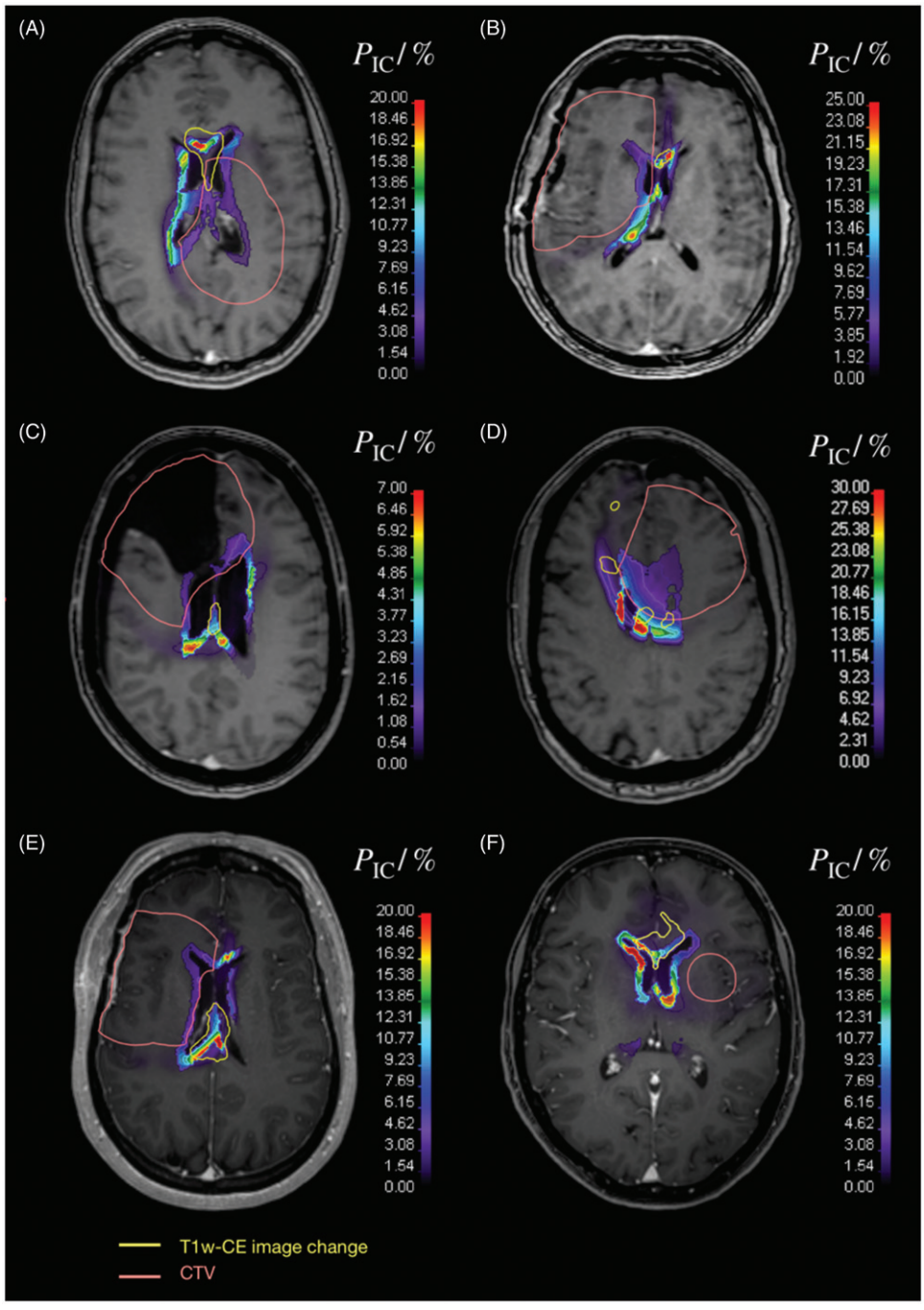

Figure 1. Predicted image change probabilities of the logistic regression model $\mathcal{M}_X$ and clinical target volume (CTV) on planning magnetic resonance images (MRI) for patients P_I–P_{VI} (A–F) containing image changes. The corresponding T1w-CE image change regions that were contoured on the follow-up MRI and deformedly co-registered to the planning MRI are shown as well as the clinical target volume (CTV).

essentially constant, the incorporation of photon patient data may help to better distinguish between the influence of LET and the PVR. However, the low to moderate intercorrelation between the PVR, LET and dose illustrates that these predictors provide independent information to modeling.

For RBE estimation, model $\mathcal{M}_{IX}$ appears most suitable because of its high cross-validated mean AUC value of 0.91, its simplicity and its potential applicability to photon patients. The magnitude of the derived RBE values corresponds to *in-vitro* data [15] and supports the postulated increased biological dose within normal brain tissue structures adjacent to the CTV [6]. Obviously, the estimated absolute RBE values depend on the selected model and hence should not be overrated, in particular, for models $\mathcal{M}_{VIII}$ and $\mathcal{M}_X$ (Figure S4). The presented methodology allows for deriving RBE from clinical data, which is the basis for biologically adapted treatment planning. An enlarged patient cohort including patients without image changes will be used to validate the clinically observed indication of a variable proton RBE.

In conclusion, the spatial distribution of late treatment-induced MR image changes in the brain following passive scattering proton therapy was highly non-uniform. A correlation with dose, LET and the PVR was shown demonstrating the relevance of variable dose-response modeling for proton

Table 1. Results of the leave-one-out cross validation with dose, LET and PVR for six glioma patients using six subsets each with five patients for model training and the remaining left-out patient for model testing.

				AUC			
Model	P1	P2	P3	Mean	Range	AIC	pR^2
M_I	D	–	–	0.65	0.58–0.76	134696	0.0238
M_{II}	LET	–	–	0.64	0.53–0.82	137106	0.0063
M_{III}	PVR	–	–	0.75	0.52–0.94	115670	0.1617
M_{IV}	D x PVR	–	–	0.76	0.50–0.95	115706	0.1614
M_V	D	PVR	–	0.80	0.62–0.82	113789	0.1753
M_{VI}	D x LET	–	–	0.88	0.86–0.91	116906	0.1527
M_{VII}	D	LET	–	0.88	0.82–0.94	119677	0.1326
M_{VIII}	D x LET	PVR	–	0.92	0.84–0.97	103926	0.2468
M_{IX}	D	LET	PVR	0.91	0.83–0.98	105437	0.2358
M_X	D	D x LET	PVR	0.91	0.84–0.97	103913	0.2468

The mean and range of the six test AUC values are reported for every modeling approach. Akaike information criterion (AIC) and pseudo R-squared (pR^2) values are shown for the corresponding logit models built on the full voxel dataset. $\mathcal{M}_{I-X}$: logistic regression models; P1-3: model predictors; AUC: area under the curve; AIC: akaike information criteria; pR^2: pseudo R-squared value; PVR: periventricular region.

therapy in the brain. The presented methodology of deriving RBE values from clinical data will develop its full potential when combined with quantitative and longitudinal functional imaging to calculate absolute RBE values for early and late brain injury.

Disclosure statement

The author(s) of this publication has research support from European Social Fund. The terms of this arrangement have been reviewed and approved by the Technical University Dresden in accordance with its policy on objectivity in research.

Funding

This research is funded by the European Social Fund and co-financed by tax funds based on the budget approved by the members of the Saxon State Parliament (Eulitz Jan, 100316833).

ORCID

P. Wohlfahrt http://orcid.org/0000-0002-2121-0934

References

[1] Baumann M, Krause M, Overgaard J, et al. Radiation oncology in the era of precision medicine. Nat Rev Cancer. 2016;16:234–249.
[2] Walker AJ, Ruzevick J, Malayeri AA, et al. Postradiation imaging changes in the CNS: how can we differentiate between treatment effect and disease progression? Future Oncol. 2014;10:1277–1297.
[3] Lambrecht M, Eekers DBP, Alapetite C, et al. Radiation dose constraints for organs at risk in neuro-oncology; the European Particle Therapy Network consensus. Radiother Oncol. 2018;128:26–36.
[4] Connor M, Karunamuni R, McDonald C, et al. Regional susceptibility to dose-dependent white matter damage after brain radiotherapy. Radiother Oncol. 2017;123:209–217.
[5] Peeler CR, Mirkovic D, Titt U, et al. Clinical evidence of variable proton biological effectiveness in pediatric patients treated for ependymoma. Radiother Oncol. 2016;121:395–401.
[6] Lühr A, von Neubeck C, Pawelke J, et al. "Radiobiology of proton therapy": results of an international expert workshop. Radiother Oncol. 2018;128:56–67.
[7] Tustison NJ, Avants B. avants Explicit B-spline regularization in diffeomorphic image registration. Front. Neuroinform 2013;7:39.
[8] Alber M, Belka C. A normal tissue dose response model of dynamic repair processes. Phys Med Biol. 2006;51:153–172.
[9] Eulitz J, Lutz B, Wohlfahrt P, et al. A Monte Carlo based radiation response modeling framework to assess variability of clinical RBE in Proton therapy. under revision.
[10] Perl J, Shin J, Schümann J, et al. TOPAS: an innovative proton Monte Carlo platform for research and clinical applications. Med Phys. 2012;39:6818–6837.
[11] Cortés-Giraldo MA, Carabe A. A critical study of different Monte Carlo scoring methods of dose average linear-energy-transfer maps calculated in voxelized geometries irradiated with clinical proton beams. Phys Med Biol. 2015;60:2645–2669.
[12] Granville DA, Sawakuchi GO. Comparison of linear energy transfer scoring techniques in Monte Carlo simulations of proton beams. Phys Med Biol. 2015;60:N283–N291.
[13] Seabold S, Perktold J. Statsmodels: econometric and statistical modeling with python. 9th Python in Science Conference. SciPy Organizers; 2010.
[14] Lühr A, von Neubeck C, Krause M, et al. Relative biological effectiveness in proton beam therapy – current knowledge and future challenges. Clin Transl Radiat Oncol. 2018;9:35–41.
[15] Chaudhary P, Marshall TI, Perozziello FM, et al. Relative biological effectiveness variation along monoenergetic and modulated Bragg peaks of a 62-MeV therapeutic proton beam: a preclinical assessment. Int J Radiat Oncol Biol Phys. 2014;90:27–35.